Available online at www.sciencedirect.com
SCIENCE DIRECT®
Journal of the European Ceramic Society 25 (2005) 1813–1818
www.elsevier.com/locate/jeurceramsoc

Kinetics and mechanism of electrolytic corrosion of titanium-based ceramics in 3% NaCl solution

Vladimir A. Lavrenko [a,*], A.D. Panasyuk [a], Martine Desmaison-Brut [b], V.A. Shvets [a], Jean Desmaison [b]

[a] *Institute for Problems of Materials Science, 3 Krzhyzhanovsky str, Kiev-142, 03680, Ukraine*
[b] *University of Limoges, SPCTS, UMR CNRS 6638, 87060 Limoges, Cedex, France*

Available online 10 February 2005

Abstract

The kinetics of electrolytic oxidation (in 3% NaCl solution at 20 °C) of TiN–AlN, TiB_2–AlN, TiB_2–TiN and $TiC_{0.5}N_{0.5}$ binary ceramics, manufactured by HIP method, were studied using a potential-dynamic method of polarization curves. For determination of oxidation mechanism, the chemical analysis concerning titanium ions state in the solution as well as an XRD, SEM and AES analyses of oxidized surface layers were used. In all the cases the oxidation of ceramics above proved to be the multistage process, the peculiarities of different stages were discussed on the base of experimental data obtained by the methods pointed out. It was shown that these ceramics are exceptionally corrosion-resistant. The rate of oxidation only slightly increases in the row: TiN–AlN → TiB_2–AlN → TiB_2–TiN → $TiC_{0.5}N_{0.5}$.
© 2005 Elsevier Ltd. All rights reserved.

Keywords: Corrosion; Films; Surfaces; Composites; TiO_2

1. Introduction

Many publications are concerned with high-temperature oxidation of multiphase non-oxide ceramic systems, such as TiB_2–AlN, AlN–SiC, Si_3N_4–TiN, etc.[1–6] However, there is only limited information about corrosion resistance of ceramic composites in solutions.[7] As high-performance structural materials, these advanced ceramics can find various applications including their use in sea water. Therefore, it was of interest to carry out the systematic study of NaCl electrochemical corrosion of TiN–AlN, TiB_2–AlN, TiB_2–TiN and $TiC_{0.5}N_{0.5}$ ceramics in terms of kinetics and reaction mechanism. The electrolyte used in this study imitates, by its composition, the marine water. For comparison, the electrolytic corrosion of a monolithic titanium diboride was also investigated in the same conditions.

2. Experimental

The TiN–AlN, TiB_2–AlN, TiB_2–TiN, $TiC_{0.5}N_{0.5}$, and TiB_2 ceramics were produced by hot isostatic pressing (HIP) without the use of additives. The powders were commercially available H. C. Starck (Grade B) powders. The HIP experiments were carried out between 1630 and 1850 °C at 195 MPa for 60–90 min. The relative densities were >99% of the theoretical ones. The microstructure and phase composition of both initial samples and specimens after anode oxidation were studied by SEM and XRD methods, the XRD analysis has been carried out using a DRON-3 M device (CuK_α radiation). The anodic oxidation kinetics of the above ceramics by a 3% sodium chloride solution containing Mg^{2+} ions as additive were investigated at 20 °C by potential-dynamic method. The polarization curves[8] were recorded using a P 5848 potentiostat device. The rate of potential evolution was 0.5 mV/s. A platinum plate was used as the cathode of the electrochemical cell, and Ag/AgCl/KCl standard electrode was used as a comparative electrode. In this paper all the potentials are given in relation to the chloride–silver electrode.

* Corresponding author.
E-mail address: lavrenko@svitonline.com (V.A. Lavrenko).

0955-2219/$ – see front matter © 2005 Elsevier Ltd. All rights reserved.
doi:10.1016/j.jeurceramsoc.2004.12.014

The amount of titanium in Ti(III) and Ti(IV) states, i.e. Ti^{3+} and TiO^{2+} ions, in the electrolyte for the different polarization stages of titanium compounds dissolution was determined by chemical analysis. The total content of titanium in the solution was determined by extraction-spectrophotometric method as described in.[9] At $1 < pH < 3$, Ti forms with pyrocathehine (H_2Pct) and amide of adamantylcarbonic acid $C_{10}H_{15}CONH_2$ (Ad) a complex compound $TiOH(HPct)_3Ad_2$ which is easily extracted by chloroform. The curves of light absorption of chloroform extracts are characterized by one absorption band with a maximum at $\lambda = 410$ nm. The molar absorption coefficient $E = 10{,}000$. Then, 10 cm^3 of solution obtained after anodic dissolution of titanium-containing compounds were put into a measuring retort of 25 cm^3. Then, 8 cm^3 of 1 M pyrocathehine solution were added, the acid presence being controlled by pH-metry. The obtained solution was extracted by 10 cm^3 of 0.1 M chloroform solution of an amide (Ad). The optic density of the extracted solution was measured at $\lambda = 410$ nm in the quarts cell (layer thickness of 1 cm) using a SF-4A spectral-photometer. The titanium content was determined by using a calibrating diagram. The sensitivity of method was 0.2 μg Ti/cm^3, the relative error of titanium determination being 1–5%. A presence of Ti^{3+} ions was determined—at the simultaneous presence of Ti(IV)—by reaction of its interaction with biacetylacetone–ethylene–diamine. Hereby, a pink complex compound of trivalent titanium is formed.[10] The tetravalent titanium does not interact with this reagent.[11] So, the concentration may be calculated following the equation:

$$C_{Ti(IV)} = C_{Ti\ total} - C_{Ti(III)} \quad (1)$$

Before the electrolytic oxidation, a partial sample surface was subjected to a cathodic treatment in the same electrolyte, in order to clean it. Indeed, one can expect[12] that the chemically adsorbed oxygen on the surface has to be in situ reduced by hydrogen atoms under a deep cathodic polarization (potentials up to −1.6 V).

The AES analysis of initial samples and of their oxidized surfaces at different depth—up to 200 nm (the etching was done by Ar^+ ion bombardment)—was carried out using a JEOL JUMP-10S device. The results obtained were quantitatively treated to identify the layer composition.

3. Results and discussion

It was established that, on the sample surfaces including initial polished surfaces, there was, a priori, a thin layer of adsorbed oxygen that partially slowed down the sample oxidation in 3% NaCl solution. The effect of sample preparation, polishing and hydrogen treatment on the corrosion rate is shown in Figs. 1–3.

Along with the corrosion behavior of multiphased ceramics, for a comparative analysis, the titanium diboride anodic polarization curve is presented. In all the cases the hysteresis of straight and reciprocal runs of the cathode polarization curves corresponds to the hydrogen treatment. After this treatment, the samples are oxidized more rapidly than after polishing. Meantime, the $TiC_{0.5}N_{0.5}$ sample without treatment proved to be the most corrosion-resistant in comparison with both other preliminarily treated samples, obviously, because of the high value of the oxygen adsorption energy on its surface (Fig. 3). By comparing the Figs. 1–3, the largest thickness of oxygen adsorption film is obtained for TiB_2–AlN ceramics, the lowest one for the titanium carbonitride material.

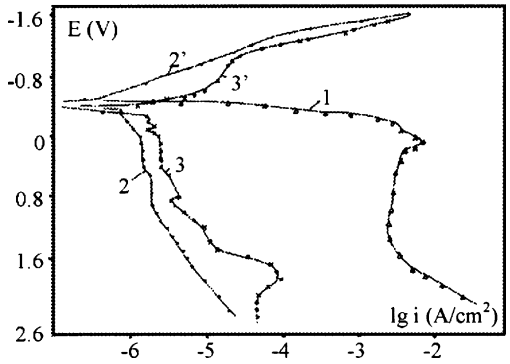

Fig. 1. Anodic polarization curves: (1) TiB_2 sample; (2) TiB_2–AlN sample after polishing; (3) TiB_2–AlN sample after hydrogen treatment; (2′) straight run cathodic curve; (3′) reciprocal run cathodic curve.

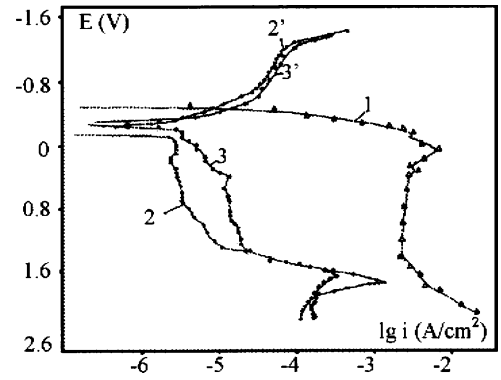

Fig. 2. Anodic polarization curves: (1) TiB_2 sample; (2) TiB_2–TiN sample after polishing; (3) TiB_2–TiN sample after hydrogen treatment; (2′) straight run cathodic curve; (3′) reciprocal run cathodic curve.

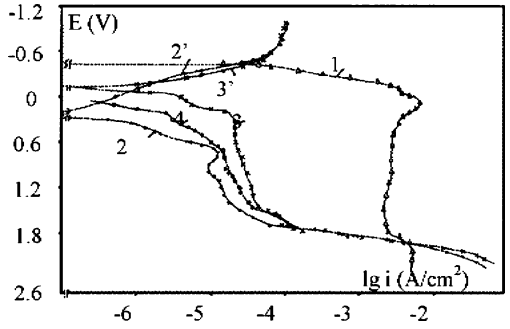

Fig. 3. Anodic polarization curves for: (1) TiB_2 sample; (2) $TiC_{0.5}N_{0.5}$ sample without treatment; (3) $TiC_{0.5}N_{0.5}$ sample after hydrogen treatment; (4) after polishing; (2′) straight run cathodic curve; (3′) reciprocal run cathodic curve.

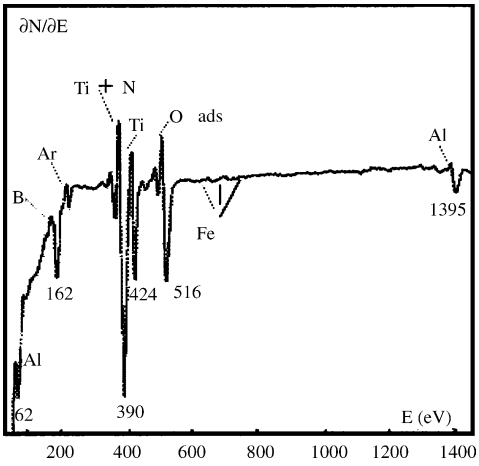

Fig. 4. Auger spectrum of initial TiB_2–AlN sample.

The presence of initial oxide layer on the surface of TiB_2–AlN sample is confirmed (Fig. 4). In this case, the quantitative calculations of AES data showed that the $O/\sum(Ti + B + Al + N)$ molar part ratio was equal to ~5/1. This result supposes the presence of only one chemically bonded layer on the surface.

It was established that in all the cases the corrosion process of the studied ceramics by the 3% NaCl solution is a multistep one (Figs. 5 and 6).

After an initial anodic dissolution including formation of TiO^{2+}, Ti^{3+} and $BO_3{}^{3-}$ ions into the solution, the formation of partially protective layers (TiN_xO_y, $TiC_xN_yO_z$ and TiO_2 rutile) can take place, these layers slow down the dissolution of the composite components.

In the case of TiN–AlN ceramics, no dissolution at all occurs in a potential range from 0.2 till 1.0 V (Fig. 5, curve 3). Then, up to 1.1 V, the dissolution of titanium nitride occurs at a very small rate with transfer of TiO^{2+} ions into solution following Eq. (2):

$$2TiN + 2H_2O = 2TiO^{2+} + 4H^+ + N_2 + 8e \quad (2)$$

From 1.1 to 1.4 V, the formation of thin TiO_2 film is observed on the sample surface by XRD analysis. In the potential range of 1.45–1.90 V the transfer of Ti^{3+} ions into solution takes place. At the final oxidation stage, at first the formation of γ-$Al(OH)_3$ (bayerite) and then of aluminum oxide-hydroxide AlO(OH) appears, first of all, due to the electrochemical evolution of oxygen on an anode in the atomic state at this polarization stage (Eqs. (3–5)):

$$2H_2O = 4H^+ + O_2 + 4e \quad (3)$$

$$2AlN + 3O + 3H_2O = 2Al(OH)_3 + N_2 \quad (4)$$

$$2AlN + 3O + H_2O = 2AlO(OH) + N_2 \quad (5)$$

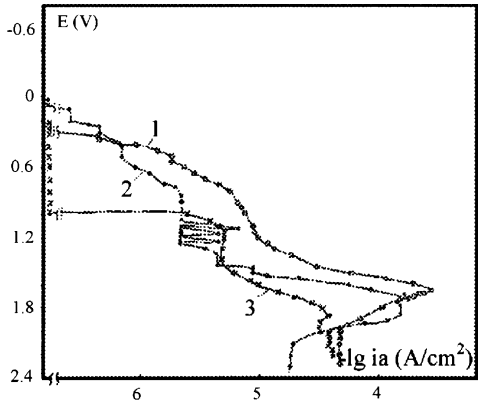

Fig. 5. Anodic polarization curves for the ceramic samples (without preliminary treatment): (1) TiB_2–TiN; (2) TiB_2–AlN; (3) TiN–AlN samples.

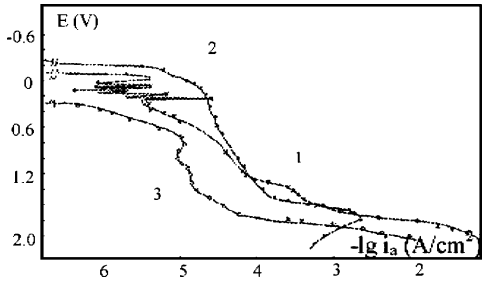

Fig. 6. Anodic polarization curves for the ceramic samples: (1) TiC; (2) TiN; (3) $TiC_{0.5}N_{0.5}$.

The Auger spectrum of initial TiN–AlN sample is presented in Fig. 7a. It was established by AES analysis that in the outer part of the oxide film (~10 nm thick) formed on the oxidized TiN–AlN ceramics (Fig. 7b), the O/Al ratio was equal to 2/1 which corresponds to the presence of the AlO(OH) phase. Only traces of TiO_2 were found. The intermediate film layer (~10 nm thickness) contains bayerite γ-$Al(OH)_3$ and rutile TiO_2 simultaneously with non-oxidized AlN and TiN grains. The calculations of Auger data enabled

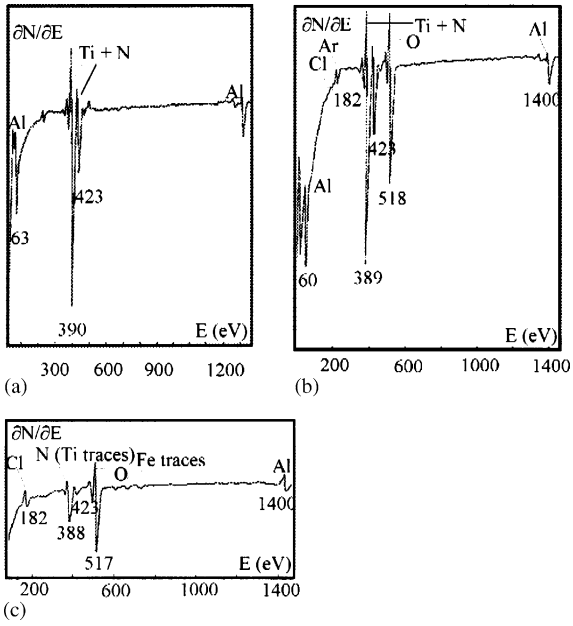

Fig. 7. Auger spectra of oxidized TiN–AlN sample: (a) external film layer; (b) intermediate layer; (c) inner layer.

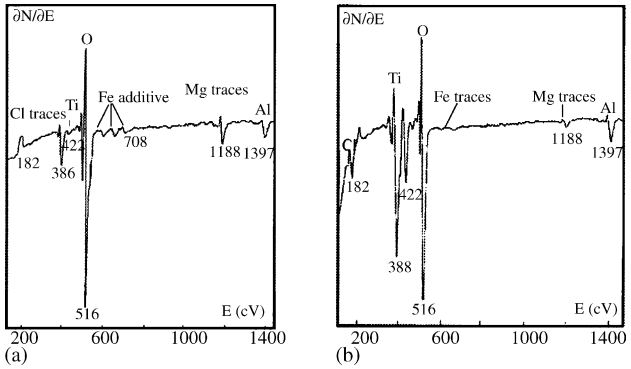

Fig. 8. Auger spectra of oxidized TiB_2–AlN sample: (a) outer oxide layer; (b) inner oxide layer.

to conclude that this layer contained less than 1/3 of oxidized AlN and less than 1/2 of oxidized TiN (Fig. 7c). Concerning the inner layer, the rutile TiO_2 is the main phase. The microstructure of oxidized TiN–AlN surface (Fig. 8a) is uniformly and finely dispersed.

Within the potential range 0.05–0.80 V, some similarities appear between TiB_2–AlN and TiN–AlN composites (Fig. 5). The transfer of both Ti^{3+} ions and boric acid into solution takes place (Eq. (6)):

$$TiB_2 + 6H_2O = Ti^{3+} + 2H_3BO_3 + 6H^+ + 9e \quad (6)$$

At a potential of 0.8 V, the formation of a non-stable rutile TiO_2 film[13] is observed:

$$TiB_2 + 8H_2O = TiO_2 + 2H_3BO_3 + 10H^+ + 10e \quad (7)$$

Then, at more positive anodic potentials, from 1.4 to 1.8 V, the reactions (3) and (4) occurs. A gel-like amorphous aluminum hydroxide is formed. At higher values, from 1.85 to 2.05 V, the sample corrosion is slowed down due to the crystallization (precipitation) of hydroxide and the formation of aluminum hydroxide γ-$Al(OH)_3$. Then, the measured current density increases, and on the last oxidation stage the aluminum hydroxide-oxide film is finally formed (see Eqs. (3) and (5)).

According to AES data (Fig. 8), an approximately 30 nm thick double layered oxide film is formed on the TiB_2–AlN sample. A thin (<15 nm) outer layer consists of a mixture of γ-$Al(OH)_3$ (largest amount) and AlO(OH) (Fig. 8a). Hereby, the ratio Al/O is equal to 12.3/35.6, i.e. ∼1/2.8. In this case, probably at potentials greater than 2.3 V, the formation of magnesium titanate Mg_2TiO_4 and sodium titanate Na_4TiO_4 traces becomes possible, according to Eqs. (8) and (9) (Fig. 8):

$$2Mg^{2+} + TiO_2 + 4H_2O = Mg_2TiO_4 + 8H^+ + O_2 + 4e \quad (8)$$

$$4Na^+ + TiO_2 + 4H_2O = Na_4TiO_4 + 8H^+ + O_2 + 4e \quad (9)$$

It must be noted that in the initial electrolyte of composition close to the marine water, a small amount of Mg^{2+} ions is present. This was proved by chemical analysis.

The composition of the inner oxide layer (Fig. 8b) corresponds to O/Al/Ti = 34/17/11 molar ratio. This layer consists of TiO_2, AlN and γ-$Al(OH)_3$, the TiO_2 content being approximately three times higher than the $Al(OH)_3$ one. It must be noted that these results are entirely consistent with XRD data.

Resulting from electrolytic oxidation, a large-dispersion oxide film is formed. This film contains AlO(OH) as small gray grains which have grown out of the great γ-$Al(OH)_3$ grains of different gray color. In addition, on the surface, the presence of a small amount of white rutile TiO_2 particles of irregular shape is noticed.

In the case of TiB_2–TiN corrosion, it was established (Fig. 5) that at first, the oxidation mechanism may be defined by the reactions (6) (polarization range 0.3–0.8 V) and (7) (polarization range 0.8–1.2 V), respectively. The formation of TiN_xO_y has also occurred, especially between 0.35 and 0.60 V. Then, in the potential range of 1.2–1.6 V, the anodic dissolution of TiN which takes place is accompanied by the transfer into the solution of titanium in the Ti(IV) state, according to Eq. (2).

Finally, from 1.60 till 1.95 V, the corrosion rate slows down due to the formation on the surface of a rutile film, in accordance to Eq. (10):

$$2TiN + 4H_2O = 2TiO_2 + 8H^+ + N_2 + 8e \quad (10)$$

The final oxidation stage for TiB_2–TiN ceramics, at potentials >2.0 V, corresponds to the sodium and magnesium titanates formation, according to Eqs. (8) and (9).

As the AES data testify, the oxide film formed on TiB_2–TiN surface consists of three layers: a very thin and dense outer layer which contains Na_4TiO_4 and Mg_2TiO_4, a very thin intermediate rutile TiO_2 layer and an inner thick layer forming a TiN_xO_y film.

The corrosion mechanism of $TiC_{0.5}N_{0.5}$ sample essentially differs from the behavior of the three previous ceramic composites. At a potential range from 0.3 to 0.7 V, the sample partially dissolved at a rather small rate, with formation of TiO^{2+} ions (Eq. (11), Fig. 6):

$$4TiC_{0.5}N_{0.5} + 4H_2O = 4TiO^{2+} = 8H^+ + 2CO_2 + N_2 + 16e \quad (11)$$

Then a three-layered oxide film is formed on the surface, this film being protective up to a potential $E = 1.4$ V. In accordance with AES data (Fig. 9), the inner scale layer is the thinnest one (∼20 nm). According to the quantitative calculations of the spectrum obtained (Fig. 9a), the ratio of corresponding molar parts of Ti/C/N/O elements in this layer is equal to 10/3/3/4. This ratio is consistent with the formula composition of $TiC_{0.3}N_{0.3}O_{0.4}$.

The intermediate scale layer (thickness ∼30 nm) is composed of the TiO lower oxide of golden-yellow color (the Ti/O ratio is close to 1/1, Fig. 9b) while the white 50 nm external layer (Ti/O ∼ 1/2, Fig. 9c) is composed of rutile TiO_2

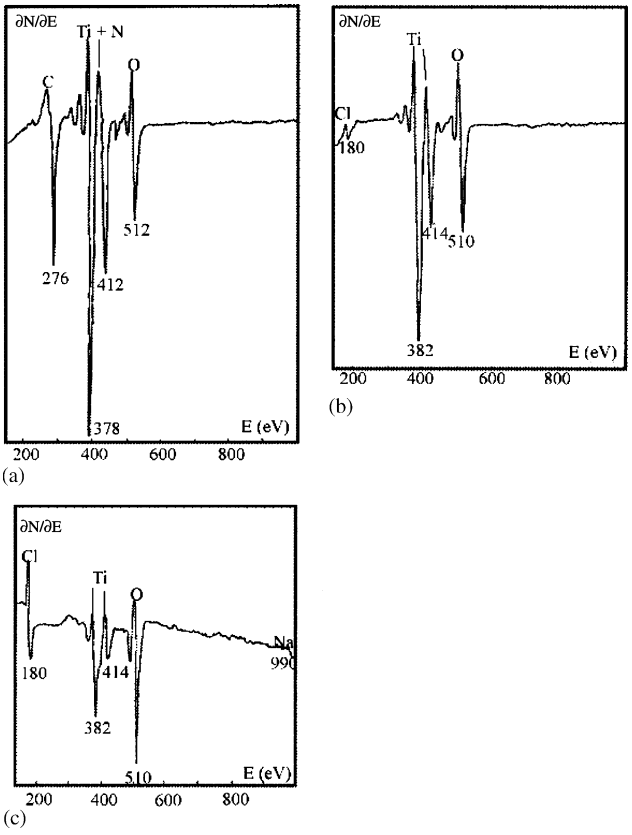

Fig. 9. Auger spectra of $TiC_{0.5}N_{0.5}$ oxidized sample: (a) inner layer; (b) intermediate layer; (c) outer layer.

(Eq. (12)):

$$4TiC_{0.5}N_{0.5} + 12H_2O = 4TiO_2 + 24H^+ + 2CO_2 + N_2 + 24e \quad (12)$$

So, the sequence of the different oxide layers formation on the titanium carbonitride $TiC_{0.5}N_{0.5}$ sample by the electrochemical process is $TiC_{0.3}N_{0.3}O_{0.4} \rightarrow TiO \rightarrow TiO_2$. All these layers, to some extent, protect the sample from the further corrosion. One can see in Fig. 10 the sharp interface

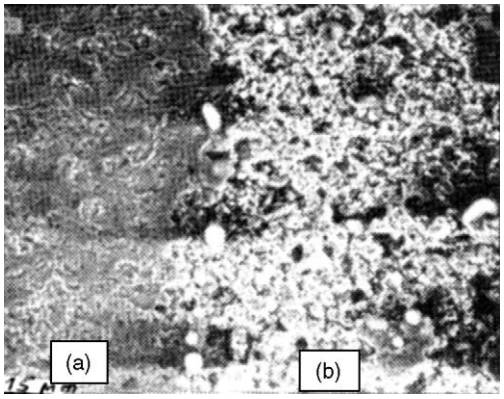

Fig. 10. Microstructure of $TiC_{0.5}N_{0.5}$ initial surface (a) and oxidized one (b).

border between an initial $TiC_{0.5}N_{0.5}$ sample and its oxide film.

So, the corrosion resistance in 3% NaCl solution of all above ceramics, prepared by HIP method, is exceptionally high. Under not too high anodic potentials, their corrosion resistance only slightly decreases in the row: (TiN–AlN) → (TiB_2–AlN) → (TiB_2–TiN) → $TiC_{0.5}N_{0.5}$. However, in all the cases, the oxidation rate for samples of such binary systems proved to be approximately by three orders lower than that of titanium diboride. Moreover, the ceramics studied have a corrosion rate by three-four orders lower than a majority of metallic materials (low carbon steels, stainless steels, etc.). Therefore, these ceramics may be recommended as high-performance materials for marine water.

4. Conclusion

The electrolytic corrosion of titanium-based materials (TiN–AlN, TiB_2–AlN, TiB_2–TiN, and $TiC_{0.5}N_{0.5}$ ceramics) in 3% NaCl solution is a multistep process. After an initial anodic dissolution, with transfer of Ti^{3+}, TiO^{2+} ions and H_3BO_3 into the solution, the formation of TiN_xO_y, $TiC_xN_yO_z$ or TiO_2 (rutile) partially protecting layers takes place; the latter oxide slows down the dissolution of the composites.

At low anodic potentials, their corrosion resistance only slightly decreases in the sequence: (TiN–AlN) → (TiB_2–AlN) → (TiB_2–TiN) → $TiC_{0.5}N_{0.5}$. At high anodic potentials, the TiN–AlN and TiB_2–AlN ceramic composites behave in a similar way. The outer protective layer which is formed on the surface proved to be a mixture of γ-$Al(OH)_3$ and AlO(OH) phases. On the surface of oxidized TiB_2–TiN ceramics (at potentials greater than +2.0 V), an extremely thin titanate layer containing both Na_4TiO_4 and Mg_2TiO_4 was detected by AES.

Concerning the carbonitride $TiC_{0.5}N_{0.5}$ ceramics, at anodic potentials up to +1.8 V, a rutile TiO_2 film is found on the surface which presents less protective properties.

Consequently, it is shown that the corrosion resistance of the above binary ceramics in 3% NaCl solution is exceptionally high. The electrolytic corrosion rate of these composites is by three-four orders lower than that of a majority of metallic materials (low carbon steels, stainless steels, etc.).

References

1. Schneider, S. V., Desmaison-Brut, M., Gogotsi, Y. G. and Desmaison, J., *Key Eng. Mater.*, 1996, **113**, 49.
2. Lavrenko, V. A., Desmaison-Brut, M., Panasyuk, A. D. and Desmaison, J., *J. Eur. Ceram. Soc.*, 1998, **18**, 2339.
3. Desmaison, J. and Desmaison-Brut, M., *Mater. Sci. Forum*, 2001, **369**, 39.
4. Gogotsi, Y. G. and Porz, F., *Corros. Sci.*, 1992, **33**, 627.

5. Graziani, T., Baxter, D. and Bellosi, A., *Key Eng. Mater.*, 1996, **113**, 123.
6. Deschaux-Beaume, F., Frety, N., Cutard, T. and Colin, C., *Mater. Sci. Forum*, 2001, **369**, 403.
7. Lavrenko, V., Shvets, V., Mosina, T. and Talash, V., In *Proceedings of the 9th Cimtec-World Ceramics Congress Ceramics: Getting into 2000's, part A*, ed. P. Vincenzini. Techna Srl, 1999.
8. Freiman, L. I., Makarov, V. A. and Bryskin, I. E., *Potentiostatic Methods in Corrosion Studies and Electric Protection*. Nauka, Leningrad, 1972.
9. Nabivanets, B. I., Knyazeva, E. N., Klimenko, E. P. and Dovgan', N. L., *J. Anal. Chem.*, 1982, **37**, 247.
10. Gambarov, D. G. and Babayev, A. K., *Organic Reagents in Analytic Chemistry, vol. 1*. Naukova dumka, Kiev, 1976.
11. Lavrenko, V. A., Lysenko, E. V. and Knyazeva, E. N., *Proc. Acad. Sci. USSR*, 1982, **267**, 1395.
12. Jones, D. A., *Principles and Prevention of Corrosion*. Prentice Hall, Upper Saddle River, USA, 1996.
13. Monticelli, C., Frignani, A., Bellosi, A., Brunoro, G. and Trabanelli, G., *Corros. Sci.*, 2001, **979**, 43.